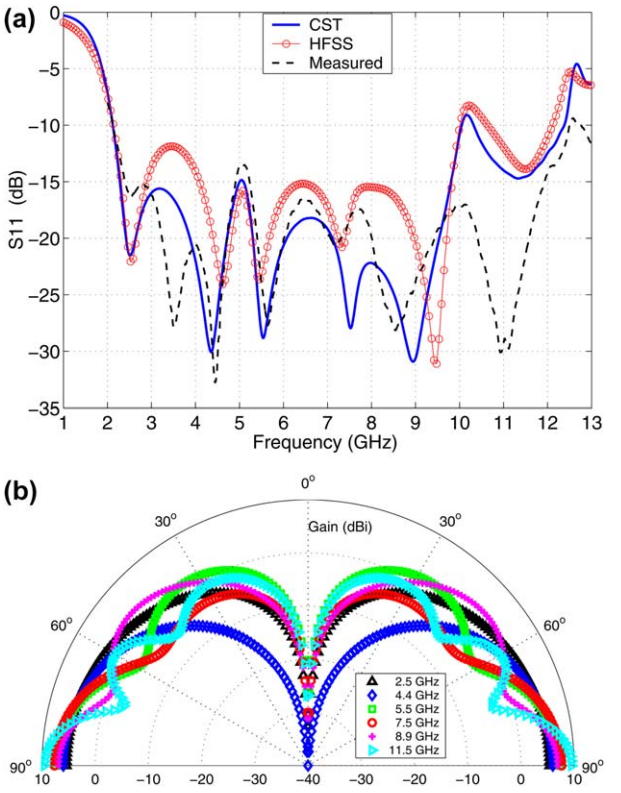

Figure 5 The third antenna with $l = 30$, $h_r = 1.5$, $r = 2$, $t = 0$. Bottom and Top DR: $a = 14$, $a_1 = 7.5$, $h = 10$, $h_1 = 5$, $b = 4.5$. (a) $|S_{11}|$ versus frequency and (b) gain pattern. [Color figure can be viewed in the online issue, which is available at wileyonlinelibrary.com]

observed at 7.5 and 10.5 GHz. This is because the DRA configuration of this antenna can be viewed as a series fed 2-element closely spaced array (with a ground plane) [10]. The fields in both DRAs at these frequencies are aligned and excited in phase. This causes a gain enhancement due to the array configuration. The measured data show that a bandwidth ratio of 140% is achieved covering the frequency range 3–17 GHz. The antenna has monopole-like radiation pattern in this frequency range. The DRAs are weakly coupled with monopole at 15 GHz causing a gain loss at this frequency. We also note that the antenna configuration proposed in this article offers better radiation performance compared to the monopole loaded by conical DRAs in a companion article [10].

Finally, a monopole of height $l = 30$ mm is used. An operating bandwidth of 143% covering the frequency range from 2 to 12 GHz is seen in Figure 5(a). In Figure 5(b) are shown monopole type gain patterns in the vertical plane. Similar resonance behavior is valid here as discussed earlier.

4. CONCLUSIONS

The hybrid monopole/DRA configuration presented in this article can easily offer more than 140% bandwidth along with monopole type radiation. An initial design procedure has also been outlined. The proposed antenna may be further optimized to obtain a better radiation performance.

REFERENCES

1. M. Lapierre, Y.M.M. Antar, A. Ittipiboon, and A. Petosa, Ultra wideband monopole/dielectric resonator antenna, IEEE Microwave Wireless Compon Lett 15 (2005), 7–9.
2. D. Guha, Y.M.M. Antar, A. Ittipiboon, A. Petosa, and D. Lee, Improved design guidelines for the ultra wideband monopole-dielectric resonator antenna, IEEE Antennas Wireless Propag Lett 5 (2006), 373–377.
3. Y.W. Chan and K.M. Luk, The small UWB hybrid antenna, Microwave Opt Technol Lett 49 (2007), 2157–2159.
4. S. Ghosh and A. Chakrabarty, Ultrawideband performance of dielectric loaded T-shaped monopole transmit and receive antenna/EMI sensor, IEEE Antennas Wireless Propag Lett 7 (2008), 358–361.
5. M.N. Jazi and T.A. Denidni, Design and implementation of an ultra-wideband hybrid skirt monopole dielectric resonator antenna, IEEE Antennas Wireless Propag Lett 7 (2008), 493–496.
6. Y.F. Ruan, Y.X. Guo, and X.Q. Shi, Double annular ring dielectric resonator antenna for ultra-wideband application, Microwave Opt Technol Lett 49 (2007), 362–366.
7. C. Ozzaim, Monopole antenna loaded by a stepped radius dielectric ring resonator for ultrawide bandwidth, IEEE Antennas Wireless Propag Lett 10 (2011), 843–845.
8. D. Guha, B. Gupta, and Y. Antar, New pawn-shaped dielectric ring resonator loaded hybrid monopole antenna for improved ultra-wide bandwidth, IEEE Antennas Wireless Propag Lett 8 (2009), 1178–1181.
9. D. Guha, B. Gupta, and Y. Antar, Hybrid monopole-DRAs using hemispherical/conical-shaped dielectric ring resonators: Improved ultra-wideband designs, IEEE Trans Antennas Propag 60 (2012), 393–398.
10. C. Ozzaim, F. Ustuner, and N. Tarim, Stacked conical ring dielectric resonator antenna excited by a monopole for improved ultrawide bandwidth, IEEE Trans Antennas Propag 61 (2013), 1435–1438.

A WIDEBAND CIRCULARLY POLARIZED METALLIC CAVITY ANTENNA FED WITH AN L-SHAPED PROBE

Longsheng Liu,[1] Yang Zhao,[2] Yue Li,[1] Zhijun Zhang,[1] and Zhenghe Feng[1]
[1] State Key Laboratory of Microwave and Communications, Department of Electronic Engineering, Tsinghua University, Beijing, 100084, China; Corresponding author: zjzh@tsinghua.edu.cn
[2] Southwest China Research Institute of Electronic Equipment, Chengdu, 610036, China

Received 22 February 2014

ABSTRACT: *In this letter, a wideband circularly polarized metallic cavity antenna is designed and fabricated. To enhance both the impedance and axial-ratio bandwidths (ARBWs), an L-shaped probe is used to produce two orthogonal TE_{111} modes for left-hand circular polarization. The measured impedance bandwidth for $S_{11} \leq -10$ dB and 3-dB ARBW were 1.72 GHz (20.6%, 7.48–9.2 GHz), and 1.5 GHz (17.3%, 7.9–9.4 GHz), respectively. The measured realized gain at broadside was 6.6–9.3 dBic over the overlapped impedance and AR bandwidth 1.38 GHz (16.1%, 7.9–9.28 GHz). The experimental results reveal that the proposed antenna is attractive for satellite communication applications due to its simple metallic structure, good performance, and strong power-handling capability.* © 2014 Wiley Periodicals, Inc. Microwave Opt Technol Lett 56:2398–2403, 2014; View this article online at wileyonlinelibrary.com. DOI 10.1002/mop.28605

Key words: *circular polarization; wideband; metallic cavity antenna; strong power-handling capability*

1. INTRODUCTION

In the last decades, new and demanding satellite applications evolved, leading to spectral congestion of low-frequency bands such as L-band (2/1 GHz) and S-band (4/2 GHz). Higher

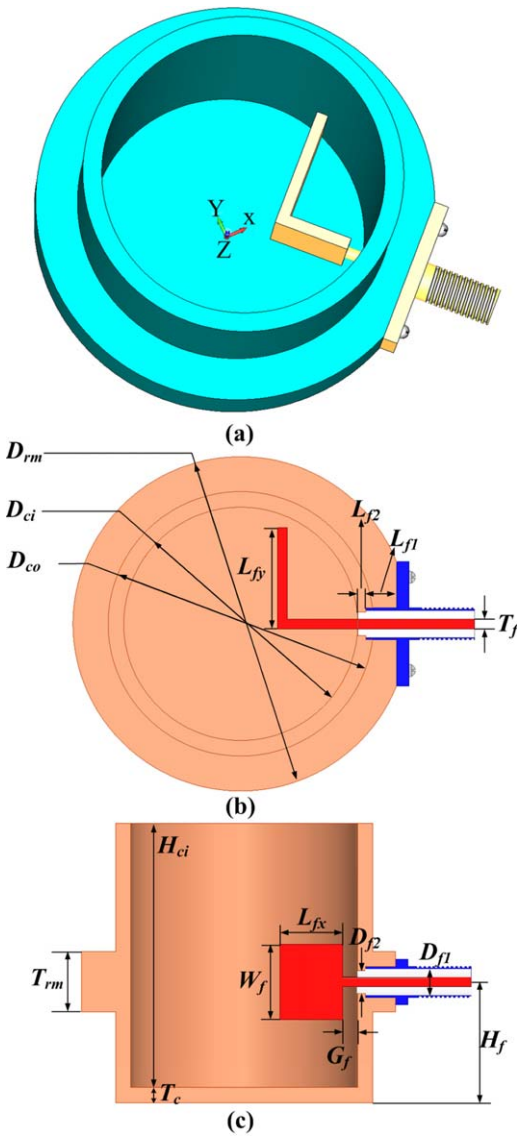

Figure 1 Geometry of the proposed antenna: (a) panoramic view; (b) sectional top view; and (c) sectional side view. [Color figure can be viewed in the online issue, which is available at wileyonlinelibrary.com]

frequency bands, namely C-band (6/4 GHz), X-band (8/7 GHz), Ku-band (14/12 GHz), and Ka-band (30/20 GHz), are becoming increasingly more urgent to obtain broader bandwidths, higher data rates, and higher gains with the same radiating aperture.

Circularly polarized (CP) antennas are highly favored in radar, satellite communications and navigation systems [1]. CP provides distinct advantages over linear polarization: it can provide greater freedom in respective orientations between a transmitter and a receiver; meanwhile, it presents better mobility and weather penetration as well as reduction of multipath interferences; particularly in satellite communications, circular polarization is capable of combating Faraday rotation caused by the ionospheric plasma containing free electrons and ions.

Various CP antennas such as microstrip patch antenna [2–4], cross dipole antenna [5], slot antenna [6], and loop antenna [7] have been developed. Generally, the operating principle of these CP antennas can be roughly classified into three categories: exciting two orthogonal field components with equal amplitude but in-phase quadrature [2, 5, 6]; utilizing sequential rotation feed configuration [3]; and taking advantage of travelling wave property of the antenna itself [7] or the feed structure [4]. However, performance of the above antennas will deteriorate severely due to fabrication errors when scaled to high-frequency bands like Ku-band and above in which the wavelengths are only a few millimeters. Moreover, their average power-handling capability is fairly limited by the heat sink capabilities of the substrate.

Cavity-backed CP antenna (CBCPA) has been widely used for satellite applications owing to its unidirectional radiation characteristic. Air filled metallic [8, 9] or substrate integrated CBCPAs [10, 11] have been proposed to realize bandwidth enhancement and high-gain performances. However, separate CP radiators are needed for CP radiation in these designs where the cavities only serve as reflectors.

Open-ended waveguide antennas with linear polarization [12, 13] are attractive candidates to realize electrically large size antenna and strong power-handling capability. A C-band CP metallic cavity antenna (MCA) with a 3-dB axial-ratio bandwidth (ARBW) of 4.7% was designed by introducing an inserted perturbation screw [14]. A ring probe-fed MCA with a largely enhanced ARBW was presented in [15]. However, an ARBW of 10.7% is still insufficient for some applications. It is shown that ARBW can be enhanced by utilizing L-shaped probe [1, 16, 17]. However, the proximity-coupled L-shaped probe in these designs only behaves as a capacitance compensating for some of the inductance by the probe itself to broaden the impedance bandwidth. ARBW is enhanced together with other techniques such as orthogonal or sequential rotation feed for radiating CP wave. A cylindrical MCA fed by an L-shaped probe with left-hand circular polarization (LHCP) is presented in this letter. L-shaped probe in the proposed design is used to excite CP wave, simultaneously improves the overlapped impedance bandwidth and 3-dB ARBW to 16.1%. The features of the proposed antenna include simple metallic structure, low cost, and easy fabrication for high-frequency satellite applications. Details of the proposed designs and the results are presented in the following sections.

2. ANTENNA DESIGN

The geometric structure of the proposed antenna is illustrated in Figure 1. As can be seen from the panoramic view shown in Figure 1(a), the antenna consists of an air-filled cylindrical cavity and an L-shaped probe. Figures 1(b) and 1(c) show the sectional top view and sectional side view, respectively. The thickened ring surrounding the outer wall of the cavity, used to fix the SMA connector, is not an intrinsical part of the design. The upper port of the cylindrical cavity is open, whereas the lower port is kept closed so as to realize unidirectional radiation.

For the proposed air-filled cylindrical waveguide cavity resonator, all the surfaces are equivalent to be perfect electrical conductors except that the upper surface is approximately assumed

TABLE 1 Dimensions of the Proposed Antenna

Parameters	*Dci*	Hci	Dco	Tc
Value (mm)	30	35	34	2
Parameters	*Drm*	*Trm*	*Hf*	*Tf*
Value (mm)	43	8	16	1.27
Parameters	*Wf*	*Gf*	*Lfx*	*Lfy*
Value (mm)	10	2	8.27	13
Parameters	*Df1*	*Df2*	*Lf1*	*Lf2*
Value (mm)	4.1	3	4	1

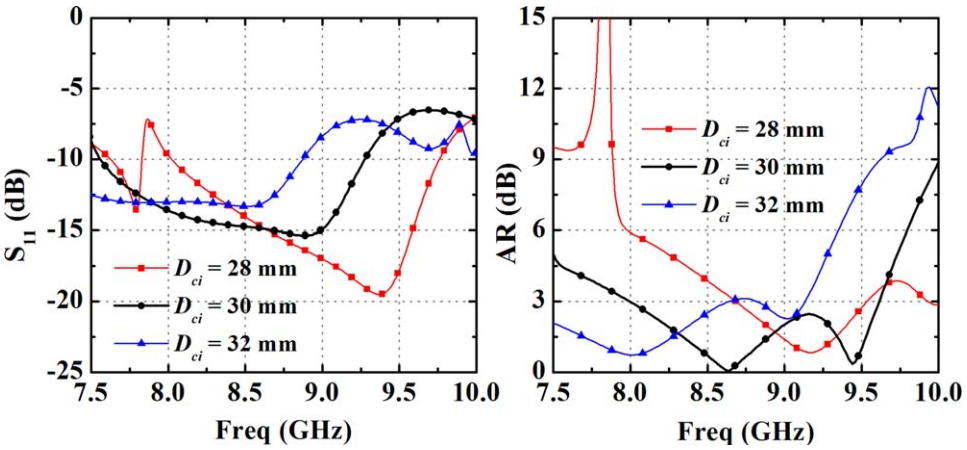

Figure 2 Effect of D_{ci} on S_{11} and AR. [Color figure can be viewed in the online issue, which is available at wileyonlinelibrary.com]

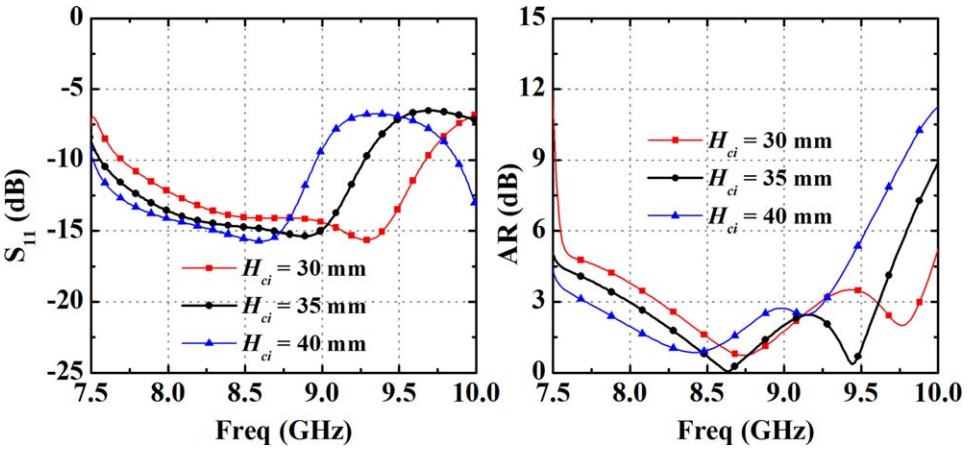

Figure 3 Effect of H_{ci} on S_{11} and AR. [Color figure can be viewed in the online issue, which is available at wileyonlinelibrary.com]

to be perfect magnetic conductors, the resonate frequency of TE_{nml} mode can be calculated by Eqs. (1) and (2) [18].

$$f_{TEnml} = \frac{c}{2\pi}\sqrt{\left(\frac{\rho'_{nm}}{R_{ci}}\right)^2 + \left(\frac{l\pi}{2H_{ci}}\right)^2} \tag{1}$$

$$J'_n(\rho'_{nm}) = 0 \tag{2}$$

where n refers to the number of circumferential (ϕ) variations, and m refers to the number of radial (ρ) variations, J_n (•) is the nth-order Bessel function of the first kind, and the prime denotes the first derivative, R_{ci} and H_{ci} are radius and height of the

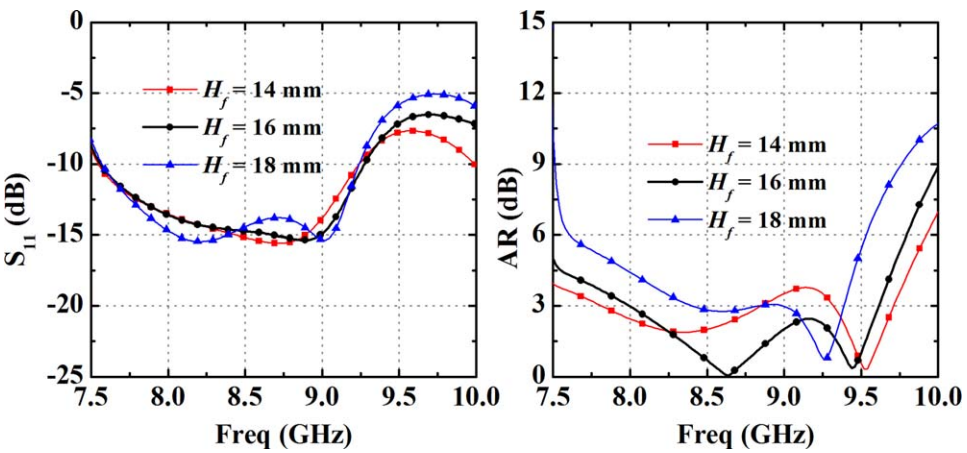

Figure 4 Effect of H_f on S_{11} and AR. [Color figure can be viewed in the online issue, which is available at wileyonlinelibrary.com]

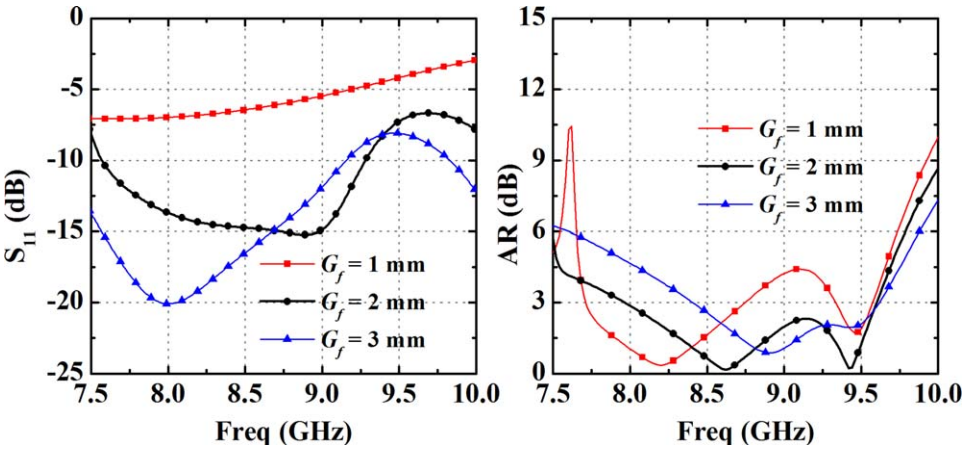

Figure 5 Effect of G_f on S_{11} and AR. [Color figure can be viewed in the online issue, which is available at wileyonlinelibrary.com]

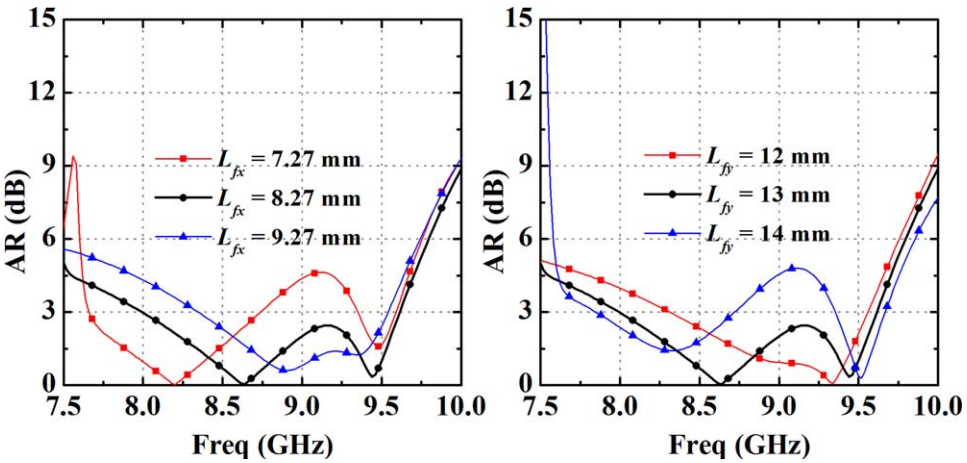

Figure 6 Effects of L_{fx} and L_{fy} on AR. [Color figure can be viewed in the online issue, which is available at wileyonlinelibrary.com]

cylindrical waveguide cavity, respectively. $fTE_{111} = 6.24$ GHz and $fTE_{211} = 9.95$ GHz are obtained by substituting $R_{ci} = 15$ mm, $H_{ci} = 35$ mm, $\rho'_{11} = 1.841$, and $\rho'_{21} = 3.054$ into (1).

The proposed antenna is designed with working frequency between the fundamental mode TE_{111} and higher order mode TE_{211} to obtain relatively pure CP pattern. Two orthogonally TE_{111} modes are generated by using an L-shaped probe. The current on the horizontal component with L_{fx} lags 90° behind that of vertical component with L_{fy}, which causes in-phase quadrature between components Ex and Ey of the electric field and produces LHCP waves at the upper open aperture, meanwhile the height of L-shaped probe W_f is carefully chosen to keep the amplitudes of Ex and Ey identical for good AR.

As can be seen from Eq. (1), the operating mode and resonant frequency are mainly determined by the dimensions of the cylindrical cavity R_{ci} and H_{ci}. The distance G_f between the L-shaped probe and the SMA connector has great influence on the impedance matching of the designed antenna. The CP purity is significantly influenced by the parameters of the L-shaped probe W_f, L_{fx}, and L_{fy}.

The proposed antenna is designed and simulated using Ansoft HFSS full-wave simulator. The optimized dimensions of the proposed antenna are shown in Table 1. The size of the radiating aperture is 30 mm (0.842 λ_0) × 30 mm (0.842 λ_0), and the overall height is 35 mm (0.982 λ_0), where λ_0 is the wavelength in free space at the center frequency 8.42 GHz.

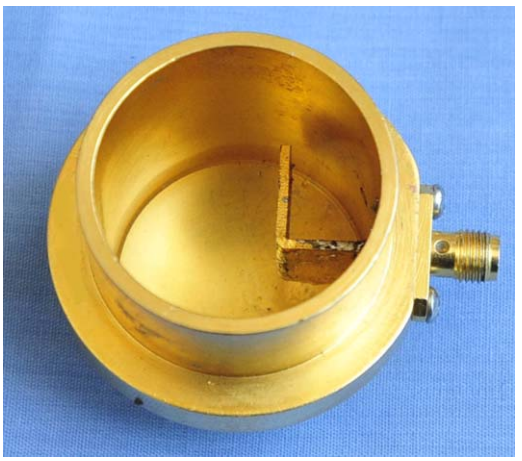

Figure 7 Photograph of the fabricated prototype. [Color figure can be viewed in the online issue, which is available at wileyonlinelibrary.com]

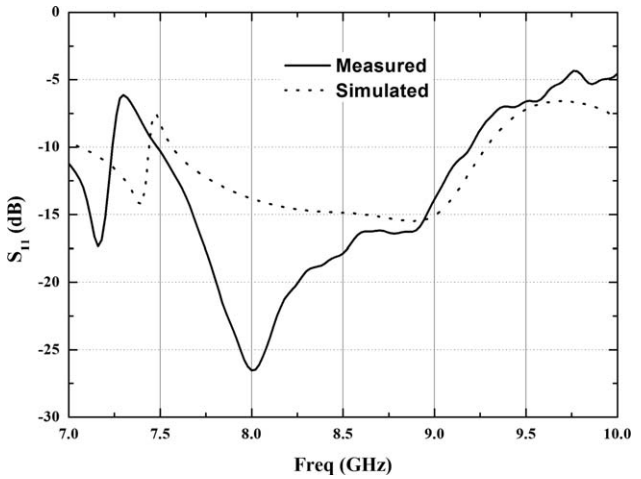

Figure 8 Measured and simulated S_{11} of the proposed antenna.

3. PARAMETRIC STUDY

Some important parameters are investigated to further understand their effects on the performance of the proposed antenna. Parametric study analysis is done on the condition of changing only one parameter once and keeping the others the same as given in Table 1.

3.1. Dimensions of Cylindrical Cavity D_{ci} and H_{ci}

The influence of the inner diameter D_{ci} and length H_{ci} of the cavity on the reflection coefficient and AR is shown in Figures 2 and 3, respectively. The dimensions of the cylindrical cavity D_{ci} and H_{ci} have a great influence on both the reflection coefficient and axial ratio. As D_{ci} or H_{ci} increases, both the center frequency of S parameter and AR shift downward.

3.2. Position of the Feed Structure H_f and G_f

In Figures 4 and 5, H_f and G_f are investigated to find their effect on the antenna performance. The height of the feed structure H_f has great influence on AR whereas almost no impact on impedance matching. It can be found that the best AR property occurred for $H_f = 16$ mm. It should be noted that both the impedance and AR property will deteriorate by greatly increasing or decreasing H_f from 16 mm.

In the proposed structure, the cylindrical probe with a length of G_f introduces an inductance that can significantly affect the reflection coefficient. Impedance matching gets worse as G_f decreases from 2 to 1 mm. Poor impedance matching has impact on the current distribution on the L-probe, therefore, AR property deteriorates to some extends.

3.3. Dimensions of L-Shaped Probe L_{fx} and L_{fy}

Figure 6 depicts the variety of impedance and AR curves when adjusting L_{fx} and L_{fy}. As can be seen from the simulation results, both L_{fx} and L_{fy} have a great influence on the axial ratio because

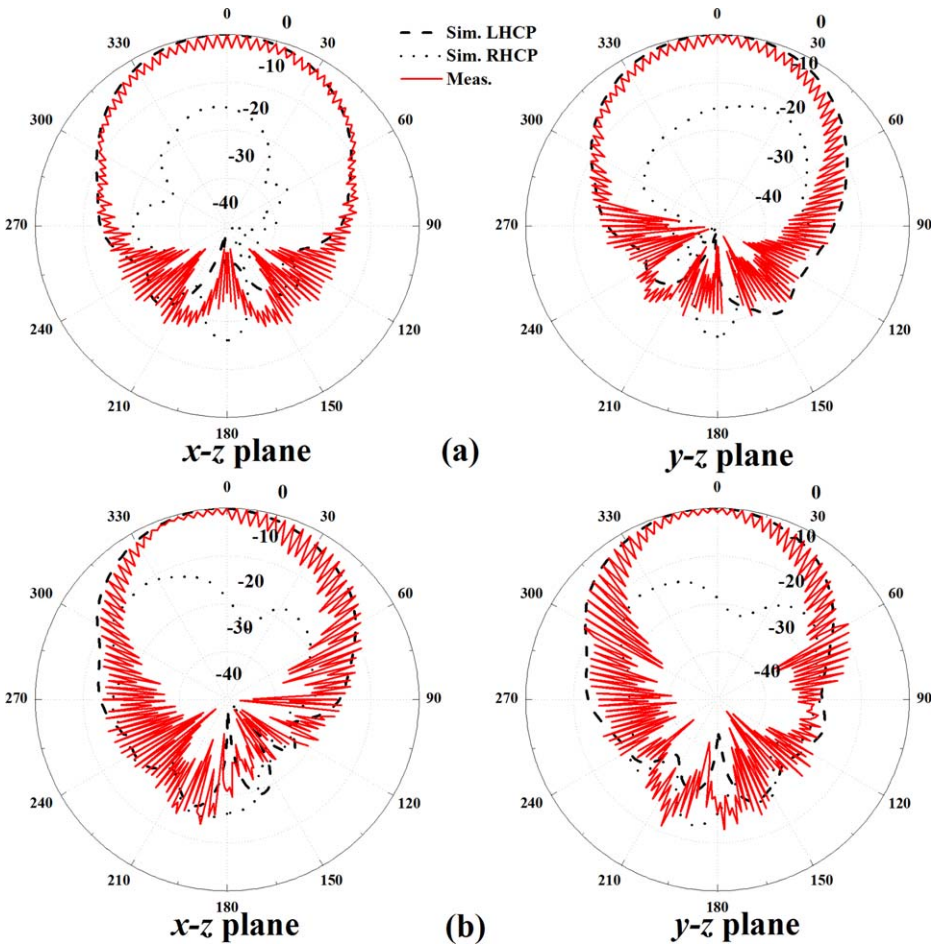

Figure 9 Measured and simulated radiation patterns of the antenna in *xz*- and *yz*-planes. (a) at 8.5 GHz and (b) at 9.4 GHz. [Color figure can be viewed in the online issue, which is available at wileyonlinelibrary.com]

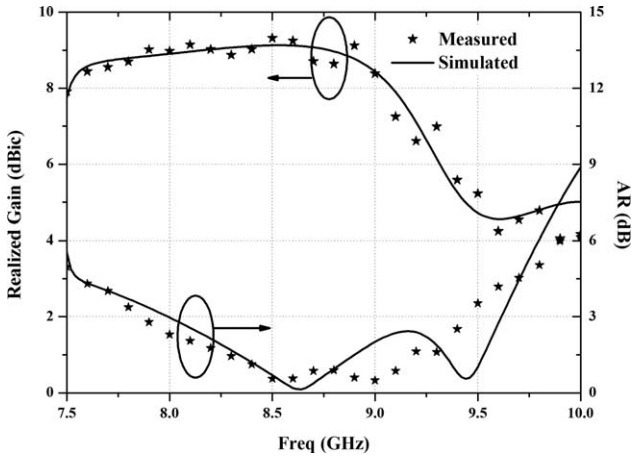

Figure 10 Measured and simulated realized gain and axial ratio at the broadside.

they both determine the phase difference between components *Ex* and *Ey* of the electric field at the desired operating frequency.

4. RESULTS AND DISCUSSION

To demonstrate the validity of the presented design strategy, as depicted in Figure 7, a prototype antenna was fabricated and measured. The reflection coefficients were obtained by a vector network analyzer Agilent ENA E8363B while the radiation patterns were measured by spinning linear method in an anechoic chamber. Simulated and measured results are given in Figures 8–10. Reasonable agreement between them could be observed. The discrepancies may be caused by the fabrication error and measurement system setup.

Both the simulated and measured *S* parameters are shown in Figure 8. The simulated and measured impedance bandwidths for $S_{11} \leq -10$ dB are 1.7 GHz (20.2%, 7.58–9.28 GHz) and 1.72 GHz (20.6%, 7.48–9.2 GHz), respectively.

Figures 9(a) and 9(b) illustrate the simulated normalized radiation patterns and measured normalized spinning linear radiation patterns in both *xz*- and *yz*-planes at 8.5 and 9.4 GHz. The difference between two adjacent values of the measured zigzag patterns represents the corresponding axial ratio while the outer profile reflects the diversity to some extents.

Figure 10 depicts the simulated and measured realized gain and AR of the proposed antenna against frequency. The simulated and measured 3-dB ARBW are 1.62 GHz (18.4%, 8–9.62 GHz) and 1.5 GHz (17.3%, 7.9–9.4 GHz), respectively. The overlapped impedance and AR bandwidth for the measured results is 1.38 GHz (16.1%, 7.9–9.28 GHz). The gain remains stable ranging from 8 to 9.3 dBic over 7.9–9.1 GHz and it begins to drop off remarkably above 9.1 GHz which is attributed to the excitation of higher order mode.

5. CONCLUSIONS

A CP MCA is presented in this letter. Broad impedance and AR bandwidths are realized by introducing an L-shaped probe. The proposed antenna can be a good candidate for satellite communication due to its structural simplicity, low production cost, and broad bandwidth.

ACKNOWLEDGMENTS

This work is supported by the National Basic Research Program of China under Contract 2013CB329002, in part by the National High Technology Research and Development Program of China (863 Program) under Contract 2011AA010202, the National Natural Science Foundation of China under Contract 61271135, the National Science and Technology Major Project of the Ministry of Science and Technology of China 2013ZX03003008-002.

REFERENCES

1. Z.-H. Wu, Y. Lou, and E.K.-N. Yung, A circular patch fed by a switch line balun with printed L-probes for broadband CP Performance, IEEE Antennas Wireless Propag Lett 6 (2007), 608–611.
2. X.Y. Sun, Z.J. Zhang, and Z.H. Feng, Dual-band circularly polarized stacked annular-ring patch antenna for GPS application, IEEE Antennas Wireless Propag Lett 10 (2011), 49–52.
3. Y. Li, Z.J. Zhang, and Z.H. Feng, A sequential-phase feed using a circularly polarized shorted loop structure, IEEE Trans Antennas Propag 61 (2013), 1443–1447.
4. K.M. Lum, T. Tick, C. Free, and H. Jantunen, Design and measurement data for a microwave dual-CP antenna using a new traveling-wave feed concept, IEEE Trans Antennas Propag 54 (2006), 2880–2886.
5. Y.-F. Lin, Y.-K. Wang, H.-M. Chen, and Z.-Z. Yang, Circularly polarized crossed dipole antenna with phase delay lines for RFID handheld reader, IEEE Trans Antennas Propag 60 (2012), 1221–1227.
6. G.H. Li, H.Q. Zhai, T. Li, L. Li, and C.H. Liang, CPW-fed S-shaped slot antenna for broadband circular polarization, IEEE Antennas Wireless Propag Lett 12 (2012), 619–622.
7. X.L. Quan, R.L. Li, and M.M. Tentzeris, A broadband omnidirectional circularly polarized antenna, IEEE Trans Antennas Propag 61 (2013), 2363–2370.
8. S.-W. Qu, C.H. Chan, and Q. Xue, Wideband and high-Gain composite cavity-backed crossed triangular bowtie dipoles for circularly polarized radiation, IEEE Trans Antennas Propag 58 (2010), 3157–3164.
9. Q. Yang, X.M. Zhang, N. Wang, X. Bai, J.Y. Li, and X.D. Zhao, Cavity-backed circularly polarized self-phased four-loop antenna for gain enhancement, IEEE Trans Antennas Propag 59 (2011), 685–688.
10. G.Q. Luo and L.L. Sun, A reconfigurable cavity backed antenna for circular polarization diversity, Microwave Opt Technol Lett 51 (2009), 1491–1493.
11. C. Jin, R. Li, A. Alphones, and X.Y. Bao, Quarter-mode substrate integrated waveguide and its application to antennas design, IEEE Trans Antennas Propag 61 (2013), 2921–2928.
12. G.-H. Zhang, Y. Fu, C. Zhu, D.-B. Yan, and N.-C. Yuan, A circular waveguide antenna using high-impedance ground plane, IEEE Antennas Wireless Propag Lett 2 (2003), 86–88.
13. A. Elsherbini and K. Sarabandi, Compact directive ultra-wideband rectangular waveguide based antenna for radar and communication applications, IEEE Trans Antennas Propag 60 (2012), 2203–2209.
14. Y. Zhao, Z. Zhang, and Z. Feng, An electrically large metallic cavity antenna with circular polarization for satellite applications, IEEE Antennas Wireless Propag Lett 10 (2011), 1461–1464.
15. K.P. Wei, Z.J. Zhang, Y. Zhao, and Z.H. Feng, Design of a ring probe-fed metallic cavity antenna for satellite applications, IEEE Trans Antennas Propag 61 (2013), 4836–4839.
16. C.R. Liu, S.Q. Xiao, Y.-X. Guo, Y.-Y. Bai, and B.-Z. Wang, Broadband circularly polarized beam-steering antenna array, IEEE Trans Antennas Propag 61 (2013), 1475–1479.
17. Y. Ding and K.W. Leung, Dual-band circularly polarized dual-slot antenna with a dielectric cover, IEEE Trans Antennas Propag 57 (2009), 3757–3764.
18. David M. Pozar, Microwave engineering, 3rd ed., Wiley, New York, NY, 2005.